



Aquatic locomotion due to a flexible foil flapping in a perfect fluid

Giorgio Graziani ¹, Damiano Paniccia ^{1,2}, and Renzo Piva ¹

Corresponding author: Giorgio Graziani, g.graziani@uniroma1.it

(Received 8 March 2025; revised 14 August 2025; accepted 16 September 2025)

Can a fish-like body swim in a perfect fluid – one that is purely inviscid and does not release vorticity? This question was raised by Saffman over fifty years ago, and he provided a positive answer by demonstrating a possible solution for an inhomogeneous body. In this paper, we seek to determine a suitable deformation for oscillatory fish swimming that enables slight locomotion in a perfect fluid, relying solely on tail flapping motion. This swimming style, typical of carangiform and thunniform species, allows for a separate analysis of the tail's interaction with the surrounding fluid. As a preliminary approach, the tail is approximated as a rigid plate with prescribed heave and pitch motions, while the presence of a virtual body placed in front is considered to evaluate the locomotion. Analytical solutions provide exact results while avoiding singular behaviour at sharp edges. A phase shift is shown to be strictly necessary for generating locomotion. A more refined approximation of a real fish is achieved by modelling the tail as a flexible foil, connected to the main body via a torsional spring with tuneable stiffness at the peduncle. While the heave motion remains prescribed, the pitch amplitude and phase are passively determined by flow interaction. A plausible solution reveals an optimal stride length as a function of dimensionless stiffness, driven by resonance phenomena. A small structural damping must be considered to induce a phase shift – essential for self-propulsion in the absence of vorticity release.

Key words: flow-structure interactions, propulsion, swimming/flying

1. Introduction

In the present paper we focus on fish-like bodies that achieve self-propulsion by flapping their tails. The rest of the body, containing the larger part of the total mass, essentially

© The Author(s), 2025. Published by Cambridge University Press. This is an Open Access article, distributed under the terms of the Creative Commons Attribution licence (https://creativecommons.org/licenses/by/4.0/), which permits unrestricted re-use, distribution and reproduction, provided the original article is properly cited.

¹Department of Mechanical and Aerospace Engineering, Sapienza Università di Roma, Via Eudossiana, 18, 00184 Roma, Italy

²Leonardo S. p. A., Piazza Monte Grappa 4, Roma 00195, Italy

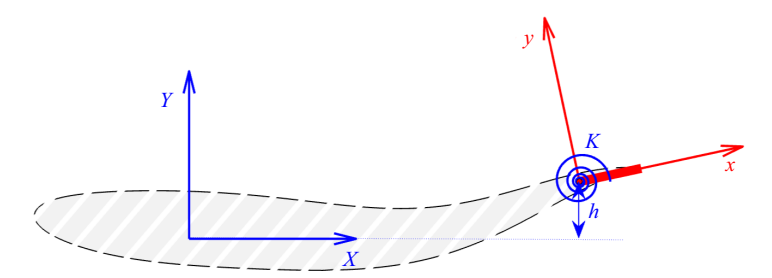


Figure 1. Sketch of the virtual body with the flat plate attached through a torsional spring. The ground frame (X-Y) and the body-fixed one (x-y) are shown.

contributes to the stability of locomotion, by keeping control of the recoil motions, while it gives rise to the major part of the resistance, which in the present study is not considered. This behaviour, characteristic of carangiform or thunniform fish, is well known in the literature as oscillatory swimming in contrast to undulatory swimming which involves the deformation of a larger portion of the body to generate propulsion.

Due to its nature, the oscillatory swimming allows us to analyse separately the fish tail as the main propulsive tool, whose interaction with the surrounding fluid was frequently studied by considering its motion under an incoming uniform stream, especially in the field of experimental investigation. In case a direct analysis of self-propulsion is believed more appropriate, simplified theoretical models are easily devised to obtain significant results in a neat form, either by analytical or by numerical methods.

For instance, in the following, we consider the motion of a virtual body (Akoz & Moored 2018, Moored & Quinn 2019, Paniccia *et al.* 2021*c*) with prescribed integral properties, at the end of which the flapping tail is attached, with its proper heave and pitch motion, see figure 1. More details are reported in the Supplementary Materials in Paniccia *et al.* (2021*c*). Within this kind of approximation, we may study the interaction with the surrounding fluid of the isolated tail, by recovering the presence of the main body only in terms of its inertial effects on locomotion, as lateral and angular recoil motions are supposed to be prevented by the prevailing size of the main body itself. In general, self-propulsion occurs when the thrust generated by the flapping tail balances the prescribed drag of the main body (Smits 2019) while in the present study both drag and thrust are null, as expected in perfect fluid.

In previous studies (Paniccia *et al.* 2021*a*, 2021*b*) we adopted this model to analyse the axial motion of fish body propelled by a flapping tail in the framework of inviscid flows in the presence of non-diffusing vorticity. As a plus, potential theory is able to identify clearly the added mass responsible for the reactive forces, as discussed in Lighthill (1960, 1969) and Wu (1961). Furthermore, the application of an unsteady Kutta condition mimicking the effect of viscosity at the trailing edge singularity implies the release of concentrated vorticity as the main mechanism for the exchange of momentum with the fluid. Particular attention was given to the different roles played by the added mass and by the vortical terms of the governing equations, but also to their couplings which have a positive influence not only on the locomotion, but also on the manoeuvrability of the fish body. See Limacher (2019) and our previous contribution on the C-start maneuver, i.e., the rapid escape motion with a C-shape bending of the swimmer (Paniccia *et al.* 2022).

The effort to extend this procedure to include flexible tails, resembling the thin tails of real fish (Quinn & Lauder 2022), led to the further modelling proposed by Moore (2014, 2015), which considers the flexibility to be fully concentrated at the leading edge by a local torsional spring with a proper stiffness, while the rest of the tail is treated as a rigid body.

The reactive forces, expressed in terms of potential flow and added-mass coefficients, have a primary role in the transfer of energy from the flexible tail to the surrounding fluid through a torsional balance equation. In general, this energy, ultimately captured by vortex shedding, plays a crucial role in generating the backward fluid momentum required for the body's locomotion in the opposite direction.

For a better comprehension of the added-mass effects, we like to consider here, as a starting point, swimming in a pure inviscid fluid able to exchange only reactive forces without any release of vorticity, that we identify as a perfect fluid following Saffman (1967). This problem has been studied by several authors, among others Childress (1981), Kelly (1998), Kelly & Murray (2000) and Kanso *et al.* (2005). A similar problem was also studied by Miloh & Galper (1993) and by Chambrion & Munnier (2011) within the framework of geometric mechanics.

The aim of the present study, about swimming in a perfect fluid, is twofold. First, by considering only the reactive forces we can precisely evaluate the added-mass terms in the solution, either for flexible or rigid tails, which should be extended afterwards to include the release of vorticity. Hence, we intend to consider the perfect fluid solution as a valuable step to obtain a reliable extension of the model to include circulatory contributions. Second, the present ideal solutions are of fundamental interest *per se*, as they address the question posed by Saffman (1967) regarding whether a fish-like body, initially at rest in an unbounded fluid, can achieve locomotion solely by undergoing periodic shape changes. The solution shown in the present paper can be quite significant for the case of homogeneous bodies. The hypothetical application for swimming in superfluids is just corroborating the above interest.

More specifically, in this paper, we apply the model to study the locomotion of a flat plate undergoing prescribed heaving motion and free to pitch about its leading edge. A torsional spring at the leading edge mimics the flexibility of the plate, influencing in an analogous way the overall performance (see Eldredge, Toomey & Medina 2010; Wan, Dong & Huang 2012; Moore 2015).

The displacement due to a full cycle of shape variation, giving rise to the body locomotion, is here obtained by the classical theoretical models frequently adopted in fluid mechanics. The same result may be seen as a geometric phase in the framework of geometric mechanics. This approach has been used to study body locomotion either for Stokes flow or for the pure potential flow of interest in the present paper. In fact, for both very low or very high values of the Reynolds number, although the physical reasons are completely different, the resulting linear equations allow us to exploit the methodology in a quite similar way to explain the locomotion in a fluid–body system with null external forces. Purcell (1977), in his seminal paper, after discussing the scallop theorem, proposed a three-link body, with two prescribed degrees of freedom, to allow for self-propulsion in the absence of external forces. Many authors followed the same track, mostly for application to Stokes flow (e.g. see Childress & Dudley 2004), but also for application to pure potential flow in a perfect fluid (e.g. Radford 1998, Mason 2003; Melli, Rowley & Rufat 2006; Ross 2006). Some works considered a comparative treatment of both cases (e.g. Hatton & Choset 2010).

In the following we will keep on with our methodology, although accounting for several of the above applications, to have a better insight and useful suggestions for a deeper physical interpretation of the results. Initially, a fully prescribed heave and pitch motion is analysed just to confirm that a small body displacement can occur even if the mean force is zero, provided an appropriate phase shift exists between the two motions. Afterwards, we focus on the main purpose of the present work, i.e., the passive behaviour of a flexible tail in pure potential flow, which, in our opinion, has not yet received sufficient attention

in either classical fluid dynamics or geometric mechanics. In the passive case the pitch motion, in terms of amplitude and phase, is not prescribed but rather is obtained by solving a torsional balance equation. This approach is shown to lead naturally to a proper phase shift once the optimal values of the ruling parameters, driven by resonance phenomena, are matched.

The paper is organised as follows: in § 2 we report the force balance for an isolated fluid-body system in an acyclic flow. We state the equations in terms of the fluid dynamic impulse and consider a two-dimensional plate to obtain the classical representation in terms of the added mass (see Batchelor 1991; Newman 2017). Once the harmonic expressions are defined to prescribe both heave and pitch motions of the tail, a first solution is obtained in § 3 to confirm that locomotion is possible in a perfect fluid even in the absence of mean forces. Section 4 is devoted to the study of the passive pitching motion: the expression of the torque balance equation and of the related fluid dynamic moment are used to derive the analytical solution in terms of pitch angle and phase; afterwards, the locomotion of the passive flapping plate is discussed together with the fundamental role of resonance. Finally some concluding remarks are presented.

2. Impulse equation and self-propulsion

Here, we adopt the approach used in our previous works, where more details are reported (see e.g. Paniccia *et al.* 2021*a*, 2021*b*), following the formulation presented in Kanso (2009). Considering the fluid–body system with V_f and V_b the fluid and body volumes, respectively, as an isolated system with no external forces acting upon it, and denoting F_b as the force acting on the body and F_f as the force acting on the fluid, the following relation can be established:

$$\boldsymbol{F}_b + \boldsymbol{F}_f = 0, \tag{2.1}$$

which expresses the total momentum conservation in integral form

$$\frac{d}{dt} \left(\int_{V_b} \rho_b \, \boldsymbol{U}_b \, dV + \int_{V_f} \rho \, \boldsymbol{U} dV \right) = 0, \tag{2.2}$$

where U_b , ρ_b are the velocity and density at any point in the homogeneous body while U, ρ refer to the same quantities in the surrounding fluid. By introducing the velocity of the body's centroid, U_{cm} , the first integral in (2.2) gives

$$\frac{d}{dt} \int_{V_b} \rho_b \, \boldsymbol{U}_b \, dV = \boldsymbol{F}_b = m_b \, \frac{d\boldsymbol{U}_{cm}}{dt}, \tag{2.3}$$

where m_b is the total mass of the body. The second integral in (2.2) represents the time variation of the fluid's momentum and can be rewritten in terms of the hydrodynamic impulse P

$$\frac{d}{dt} \int_{V_f} \rho \, \mathbf{U} \, dV = \mathbf{F}_f = \rho \, \frac{d\mathbf{P}}{dt}. \tag{2.4}$$

In a pure potential flow, the impulse P is confined to its irrotational (acyclic) component, while vorticity-related contributions are not considered. By assuming the normal outward from the body, it is defined in terms of the velocity potential ϕ as

$$\boldsymbol{P} = \boldsymbol{P}_{\phi} = -\int_{S_b} \phi \boldsymbol{n} dS. \tag{2.5}$$

Equation (2.4) can be written as

$$\mathbf{F}_f = -\rho \frac{d}{\mathrm{d}t} \int_{S_h} \phi \mathbf{n} \mathrm{d}S,\tag{2.6}$$

which aligns with the formulation by Saffman (1992). To analyse the motion of the body, we directly employ the impulse equation by combining (2.3) and (2.4) and by eliminating the time derivative (for a null initial condition), as also discussed in Kanso (2009) and Paniccia *et al.* (2021*a*)

$$m_b U_{cm} = -\rho P. \tag{2.7}$$

Now we split the impulse P into a part, P_{LOC} , due to the body locomotion and a part, P_{SH} , due to the body shape deformation. The former can be expressed through the added-mass matrix M (see also Appendix A) yielding

$$\rho P_{LOC} = MU_{cm}, \tag{2.8}$$

and (2.7) becomes

$$(m_b + \mathbf{M}) \mathbf{U}_{cm} = -\rho \mathbf{P}_{SH}, \tag{2.9}$$

which shows that, upon enforcing a periodic shape deformation given by a non-reciprocal motion of the body (as defined in Purcell 1977), we may have locomotion in the absence of mean forces or accelerations.

As previously anticipated, to analyse the self-propulsion of a fish, we model the tail as a heaving and pitching plate attached to a virtual body that contains all the mass of the system while it does not experience either applied forces or moments. This implies that: (i) the virtual body does not contribute to the impulse P in (2.7); (ii) the only source of propulsion is the oscillating tail; and (iii) the centre of mass of the system is assumed to move solely with velocity U_X in the ground reference frame, as a result of the tail's oscillations. To this aim the tail undergoes prescribed heave oscillations in the Y-direction and pitch oscillations with angular velocity $\Omega(t)e_3$ (positive counterclockwise) around the centre of rotation located at its leading edge (hereinafter denoted as LE or x_o). As a result we will obtain the locomotion of the whole system.

The impulses $P = \{P_X, P_Y\}$ appearing in (2.7) are evaluated in the ground frame. In the following, we will see that it is more convenient to use the components in the body-fixed frame $\{P_x, P_y\}$, expressed by using the rotation matrix which maps the ground to the body frame, following the approach presented in Eldredge (2019) and Limacher (2021)

$$R(\theta) = \begin{bmatrix} \cos \theta & \sin \theta \\ -\sin \theta & \cos \theta \end{bmatrix}, \tag{2.10}$$

the angle θ being assumed positive anti-clockwise. It follows that

$$\begin{bmatrix} P_X \\ P_Y \end{bmatrix} = R(\theta) \begin{bmatrix} P_X \\ P_Y \end{bmatrix} = \begin{bmatrix} P_X \cos \theta + P_Y \sin \theta \\ -P_X \sin \theta + P_Y \cos \theta \end{bmatrix}. \tag{2.11}$$

By using the rotation matrix, (2.7) becomes, in the body frame,

$$\begin{cases}
 m_b u_x = -\rho P_x, \\
 m_b u_y = -\rho P_y,
\end{cases}$$
(2.12)

where the body mass m_b is estimated as reported in Appendix B.

Let us consider a flat plate whose half-length is b = c/2 undergoing imposed harmonic heave and pitch motions $(\dot{h}e_2; \dot{\theta} e_3 = \Omega e_3)$, while its rotation centre moves with

locomotion velocity (u_x, u_y) expressed in the body frame. The outgoing normal to the upper face is $n = \{-\sin\theta; \cos\theta\} \simeq \{-\theta; 1\}$. The velocity normal to the plate is

$$U_2 = u_v + \dot{h} \cos \theta \simeq u_v + \dot{h}. \tag{2.13}$$

The relevant details to obtain the expression of the impulses in (2.12) are reported in Appendix A. By using (2.13), the impulse P_v expressed according to (A11) becomes

$$P_{\nu} = \pi b^2 \left[u_{\nu} + \dot{h} + b\dot{\theta} \right]. \tag{2.14}$$

By combining both the first (2.12) and (A11), we obtain $u_x = 0$. Finally, from the second equation in (2.12) and (2.14), the solution u_y may be obtained

$$u_{y} = \frac{-\pi \rho b^{2}}{m_{h} + \pi \rho b^{2}} \left[\dot{h} + b \dot{\theta} \right]. \tag{2.15}$$

The self-propulsion speed of the whole body is evaluated in the ground frame through the velocity $U_{cm} = \{U_X, U_Y\}$ which is expressed as

$$\begin{bmatrix} U_X \\ U_Y \end{bmatrix} = R(\theta)^T \begin{bmatrix} u_x \\ u_y \end{bmatrix} = \begin{bmatrix} \cos \theta \ u_x - \sin \theta \ u_y \\ \sin \theta \ u_x + \cos \theta \ u_y \end{bmatrix}. \tag{2.16}$$

The locomotion velocity in the body frame is given by $u_x = 0$ and u_y by (2.15), so (2.16) gives

$$U_X = \frac{\pi \rho b^2}{\left(m_b + \pi \rho b^2\right)} \left[\dot{\theta} \ b + \dot{h}\right] \sin \theta , \qquad (2.17)$$

while the U_Y component is neglected since we have assumed previously that the presence of the virtual body prevents its motion in the Y direction. It is worth highlighting that the normal component of the velocity in the body frame gives the essential contribution to obtain locomotion in the inertial frame. With respect to energy considerations, we may notice that the kinetic energy injected into the fluid by the body's deformation is essentially transferred to the locomotion kinetic energy (see Wu 1971, Kanso 2009). Since no vorticity release is included in the model, the total kinetic energy shows a periodically oscillating behaviour with a constant mean value, hence no power is transferred to the fluid and wasted into the wake. Consistently, the Froude efficiency, given in the present case by the ratio of two equal and null quantities, looses most of its interest and is not considered in the following. For a detailed description of the energy transfer process see Appendix C.

The motion of the body's centre of mass is obtained by solving $dX/dt = U_X$ and integrating in time to obtain the axial displacement for each time.

From Appendix A we may notice that, even if $P_x = 0$, this results in $F_x \neq 0$, so the force is not purely normal to the body but a tangential component arises due to the rotation of the normal vector. This aspect has been mentioned in Limacher (2021) discussing the chord-wise component of the added-mass force.

By recalling (A9) and using θ for Ω , we obtain

$$\begin{cases}
F_x = \pi \rho b^2 \dot{\theta} \left[u_y + \dot{h} + b \dot{\theta} \right], \\
F_y = -\pi \rho b^2 \left[\dot{u}_y + \ddot{h} + b \ddot{\theta} \right],
\end{cases}$$
(2.18)

where the expression of F_y may be compared with the lift reported in Theodorsen (1935). Let us underline that, by the theory of Theodorsen, we are able to compute separately the finite integral contributions given by the purely potential flow in terms of added-mass coefficients. By using the transpose of the rotation matrix (2.10) the forces in the ground

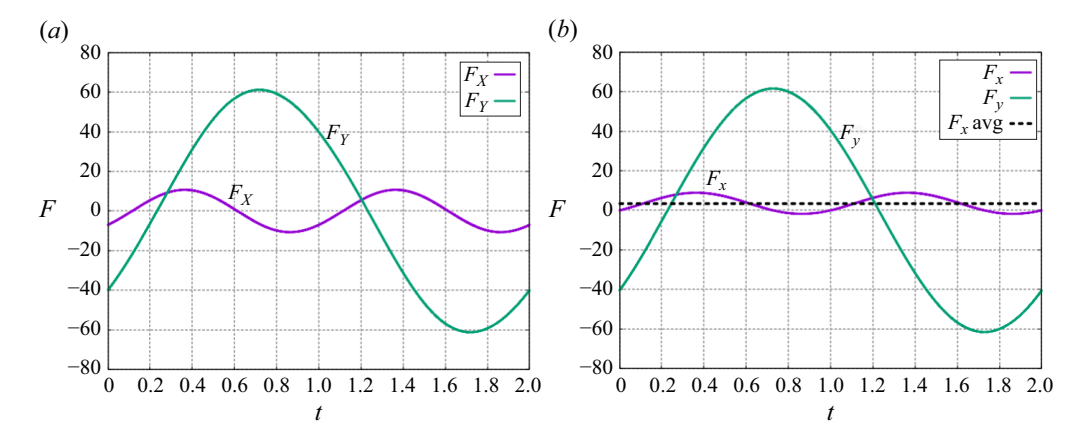


Figure 2. Time behaviour of (a) F_X and F_Y in the ground frame; (b) F_X and F_Y in the body-fixed frame (the dashed line shows the mean value of F_X) for $h_0 = 0.1$ and $\theta_0 = 10^\circ$.

and body reference frames are related by

$$\begin{bmatrix} F_X \\ F_Y \end{bmatrix} = \begin{bmatrix} \cos\theta \ F_x - \sin\theta \ F_y \\ \sin\theta \ F_x + \cos\theta \ F_y \end{bmatrix} \simeq \begin{bmatrix} F_x - \theta \ F_y \\ \theta \ F_x + F_y \end{bmatrix}.$$
(2.19)

The development of the forces during one period, both in the ground and in the body-fixed frame, is displayed in figure 2 for $h_o = 0.1$ and $\theta_o = 10^\circ$. By evaluating the average values over one period we obtain $\overline{F_X} = 0$, $\overline{F_Y} = 0$, $\overline{F_Y} = 0$ while $\overline{F_X} \neq 0$ (represented by the dashed line in the same figure).

It should be noted that the forces described above arise solely from the flapping tail, with the added-mass contribution of the virtual body excluded from the balance.

3. Locomotion for prescribed heave and pitch

As a starting point, we evaluate the motion of the body which results from prescribed heave and pitch motions. The relevant parameters appearing in what follows are: the plate thickness s^* , its length $c^* = 2 b^*$ and the densities of the fluid ρ^* and body ρ_b^* . While dimensional quantities were used up to this point, we will now distinguish between dimensional values, denoted with an asterisk (*), and their corresponding non-dimensional counterparts, which will be written without the asterisk. We define the amplitudes of the pitch and heave motions as θ_o and h_o^* , respectively, while the phase angle between them is denoted as ϕ and the oscillation frequency is $\omega^* = 2\pi f^*$. The motion of the plate is then given by

$$\begin{cases} \theta = \theta_o \sin(\omega^* t^* + \phi), \\ h^* = h_o^* \sin(\omega^* t^*). \end{cases}$$
(3.1)

To determine the mean locomotion speed, $\overline{U_X^*}$, we evaluate the average velocity over one period using (2.17). Noting that all cross-terms between heave and pitch contributions have a zero mean value, the only remaining term is $\overline{\theta \dot{h}^*} = (1/2)\omega^*\theta_o h_o^* sin(\phi)$, leading to

$$\overline{U_X^*} = \frac{1}{2} \frac{\pi \rho^* b^{*2}}{(m_b^* + \pi \rho^* b^{*2})} \theta_o \omega^* h_o^* \sin(\phi).$$
 (3.2)

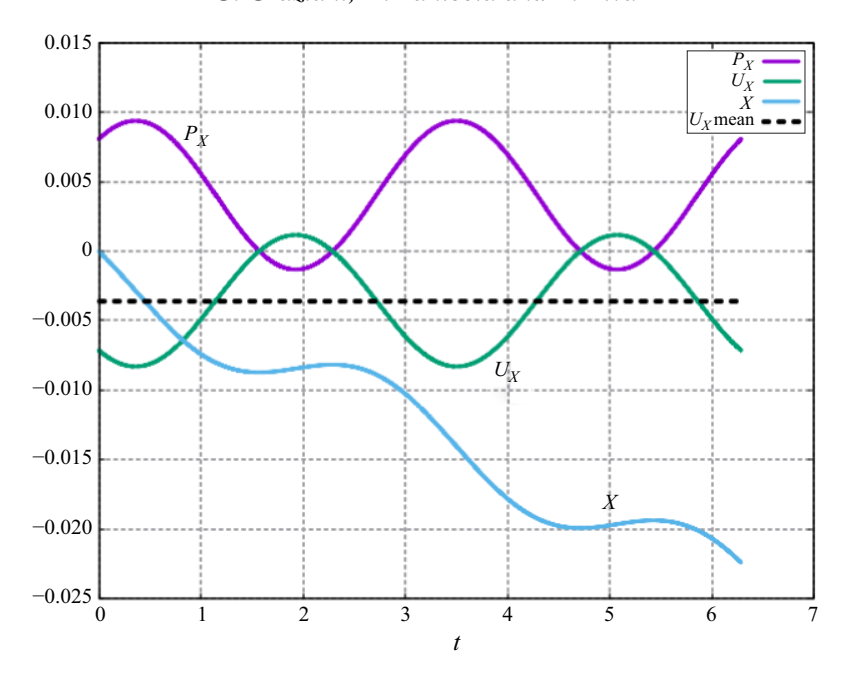


Figure 3. Time evolution of the *X*-component of impulse, velocity and displacement for heave and pitch $(h_0 = 0.1; \theta = 10^\circ; \phi = -\pi/2)$. The horizontal dashed line represents the mean value of U_X .

From (3.2) we observe two key results: (i) the sign and magnitude of the mean locomotion velocity are directly controlled by $\sin \phi$, the maximum locomotion (i.e. negative velocity) occurring for $\phi = -\pi/2$, which means that the pitch motion lags the heave motion by a quarter period, in agreement with previous findings (Quinn, Lauder & Smits 2015; Van Buren, Floryan & Smits 2018); (ii) no motion occurs when heave and pitch are in phase. Additionally, both heave and pitch must be present for locomotion. If either is absent, the body remains stationary.

By using $\omega^* = 2\pi f^*$ and $h_o^* = b^* h_o$, the average locomotion speed (3.2) can be expressed in terms of the reduced speed or the 'stride length', i.e. the non-dimensional locomotion velocity (based on the reference velocity $V_R^* = b^* f^*$) or the travelling distance measured in body lengths per second

$$U = \frac{\overline{U_X^*}}{b^* f^*} = \frac{\pi^2 \rho^* b^{*2}}{\left(m_h^* + \pi \rho^* b^{*2}\right)} \theta_o h_o \sin(\phi). \tag{3.3}$$

Figure 3 illustrates the time evolution of impulse, velocity and displacement in the X-direction for $h_o = 0.1$ and $\theta_0 = 10^\circ$ with a phase shift $\phi = -\pi/2$. The dashed line in the figure represents the mean velocity calculated from (3.2). According to the analytical expression of the mean locomotion velocity (3.2), leftward motion occurs for negative phase angles. Figure 4 shows the solution in terms of X-displacement in the ground frame as the phase shift between heave and pitch is varied from 0 to $-\pi$. In particular, we notice that the maximum displacement at the end of the cycle increases monotonically as ϕ approaches $-\pi/2$, with smaller and equal values for symmetric variations of ϕ about $-\pi/2$.

In previous studies (Paniccia *et al.* 2021c, 2023), it was shown that an appropriate phase shift can generate a travelling wave with an approximate phase velocity, $c = \omega^* h_o^* / \theta_o$, which reproduces a behaviour similar to undulatory swimming by creating a certain

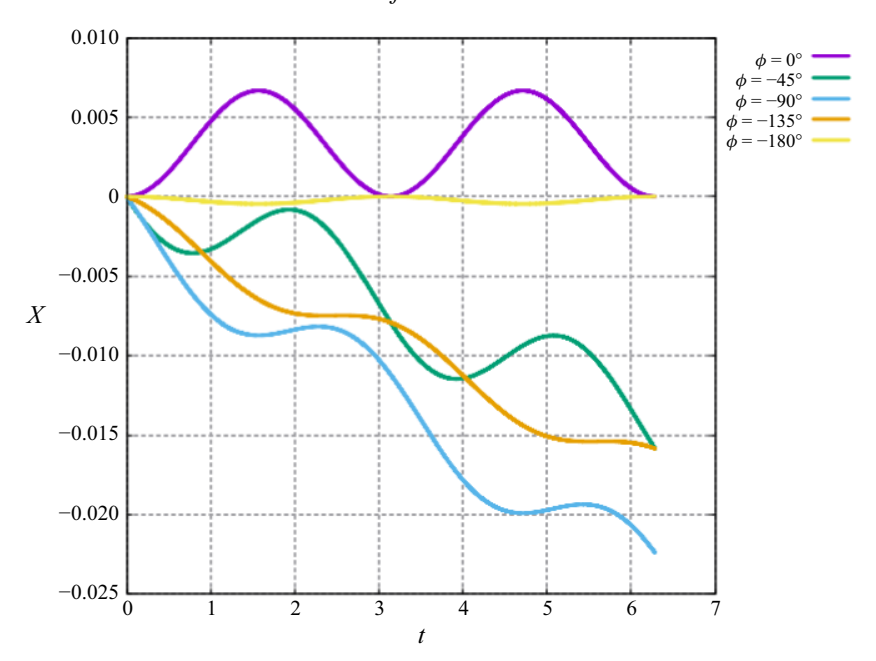


Figure 4. Temporal evolution of X displacement for heave ($h_o = 0.1$) and pitch ($\theta = 10^\circ$) with several values of the phase shift.

dissymmetry in the resulting motion. However, in the present case of a purely reactive solution, the resulting locomotion is significantly lower than the above defined c, showing a poor performance in the absence of vortex shedding.

4. Locomotion of a passive flapping plate

In this section, we analyse the fluid dynamic moment acting on a flapping plate and derive the torque balance equation, which governs the evolution of passive pitch. To represent in an efficient way a flexible plate, we will assume that the pitching motion of the plate is not prescribed but results from a torque balance involving a torsional spring at the LE (see also Toomey & Eldredge 2008; Vanella *et al.* 2009; Eldredge *et al.* 2010; Spagnolie *et al.* 2010; Zhang, Liu & Lu 2010; Moore 2014; Hang *et al.* 2022). To solve the torque balance, we must evaluate the hydrodynamic moment exerted by the surrounding fluid on the rigid body, which moves in an arbitrary manner in an unbounded fluid. For purely potential flow, only the reactive contribution is considered in the expression of the moment, while the circulatory contribution is omitted.

4.1. Fluid dynamic moment, torque balance and pitch solution

We start from the classical added-mass formulation as reported in Newman (2017), with an opposite sign convention due to the outward normal vector from the body into the fluid. We consider a two-dimensional flow field and use the position vector r' from the rotation centre at the LE of the plate. All the relevant details are reported in Appendix A.

The motion of the flat plate can be described in the body system as the superposition of the locomotion velocity components (u_x, u_y) and the prescribed heaving motion \dot{h}

$$U_1 = u_x + \dot{h}\sin\theta \simeq u_x + \dot{h}\theta \quad U_2 = u_y + \dot{h}\cos\theta \simeq u_y + \dot{h}. \tag{4.1}$$

By combining with (A17), removing quadratic terms and considering that $u_x = 0$ for a flat plate, we obtain

$$M_3 = -\pi \rho b^3 \left[\dot{u}_y + \ddot{h} + \frac{9}{8} b \ddot{\theta} \right],$$
 (4.2)

where the angular acceleration causes a moment which may be thought of as due to a virtual moment of inertia $(9/8)\rho\pi b^4$. By time differentiating (2.15) and combining with (4.2) we obtain

$$M_{3} = -\pi \rho b^{3} \left\{ \frac{m_{b}}{m_{b} + \pi \rho b^{2}} \ddot{h} + \left[\frac{m_{b}}{m_{b} + \pi \rho b^{2}} + \frac{1}{8} \right] b \ddot{\theta} \right\}. \tag{4.3}$$

Now we consider a thin foil undergoing prescribed heaving motion with a torsional spring at its LE. This set-up has been widely used in the literature as an effective model for plate flexibility due to fluid-body interaction, (see e.g. Moore 2014). Since pitching motion is not prescribed, it must be determined by solving a torsional balance equation that accounts for the fluid dynamic moment, spring restoring torque and body inertia effects.

The goal is to analyse the combined effect of forced heaving and passive pitching motion in a perfect fluid to determine to what extent self-propulsion occurs. Although approximate, this model provides some insight into the body's locomotion mechanism. A more generalised approach including the wake dynamics is addressed in an ongoing work.

A time-harmonic heaving motion, with non-dimensional amplitude $h_o = h_o^*/b^*$, is imposed at the LE of the plate. In response to this driving motion, a torsional spring with rotational stiffness k^* at the LE allows the plate to pitch passively with an assumed harmonic motion $\theta = \theta_o e^{i (\omega^* t^* + \phi)}$. The pitching motion of the plate (amplitude and phase) is not prescribed but rather is evaluated by balancing the angular moments due to the fluid (see 4.3), to the spring and to the body's inertia.

The torque balance equation governing the passive flapping motion is derived in detail in Appendix B. Below, we only report its dimensionless form and the solution in terms of pitch amplitude and phase shift between heave and pitch

$$\frac{16}{3}R\ddot{\theta} + C\dot{\theta} + K\theta = M_f + M_i, \tag{4.4}$$

where R is the body-fluid mass ratio, C and K are the dimensionless spring damping and stiffness coefficients, respectively, M_f is the dimensionless form of the fluid dynamic moment given by M_3 in (4.3) while M_i is the inertial torque due to the forced heaving.

In the torsional balance (4.4), the terms related to $\dot{\theta}$ may introduce a non-zero phase shift between heave and pitch which is required to obtain $\theta \neq 0$ and hence locomotion. The $\dot{\theta}$ term clearly appears in the spring damping while, concerning the fluid dynamic moment M_f , its presence would be associated with the circulatory component and vortex shedding.

Consistently, in the present purely reactive solution, this term is missing in the fluid dynamic moment, so the spring damping remains the only contributor to phase shift (see the second expression in (4.5) below).

Once the harmonic expressions for heave and pitch are considered and by using standard harmonic analysis, the solution for the passive pitch motion is obtained in terms of θ_o and ϕ

$$\begin{cases} \theta_o = \frac{BB h_o}{\sqrt{AA^2 + 4\pi^2 C^2}}, \\ \tan(\phi) = \frac{-2\pi C}{AA}. \end{cases}$$

$$(4.5)$$

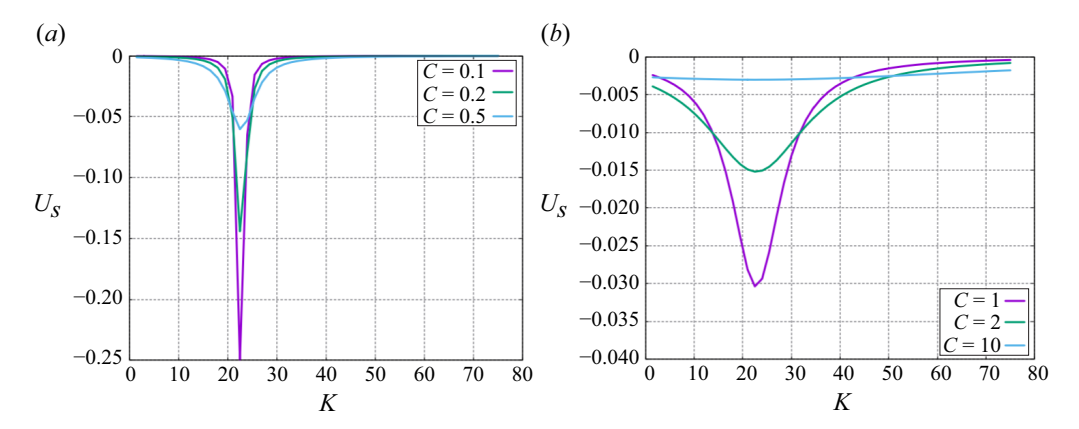


Figure 5. Behaviour of the mean self-propulsion speed U_s as a function of K ($h_o = 0.1$) for different values of the spring damping coefficient C: C = 0.1, 0.2, 0.5 (a); C = 1, 2, 10. (b).

This solution is expressed in terms of the coefficients provided in Appendix B: BB, which depends on the mass ratio R, and AA, which is function of the mass ratio as well as of the spring stiffness K. For the reader's convenience, we report below their expressions

$$BB = 16 \pi^2 R \left[\frac{4R + 2\pi}{4R + \pi} \right] \qquad R = \frac{s^* \rho_b^*}{c^* \rho^*}, \tag{4.6}$$

$$AA = -4\pi^2 \left[\frac{16}{3}R + \frac{\pi}{4} \left(\frac{36R + \pi}{8R + 2\pi} \right) \right] + K = -4\pi^2 A_1 + K.$$
 (4.7)

As clearly appears from (4.5), no pitch may occur without heave, i.e. if we have $h_o = 0$ it follows also that $\theta_o = 0$. Moreover, the solution gives $\phi = \pm \pi/2$ for AA = 0, i.e., for a given relation between the mass ratio and the spring stiffness, which, as shown below, is related to the resonance frequency. In this condition the larger energy transfer is obtained, maximising locomotion, which still remains quite small.

4.2. Swimming speed and natural frequency

Once the pitch angle and phase have been evaluated through (4.5), then the mean locomotion speed $U_s = \overline{U_X}$ may be evaluated. By using the above introduced non-dimensional quantities, the first in (3.2) gives

$$U_{s} = \frac{\overline{U_{X}^{*}}}{h^{*} f^{*}} = \pi (1 - CC)\theta_{o} h_{o} \sin(\phi) = \frac{\pi^{2}}{4 R + \pi} \theta_{o} h_{o} \sin(\phi), \tag{4.8}$$

where the coefficient *CC*, depending on the mass ratio only, is reported in (B7) in Appendix B.

The above reported solution shows that: (i) no self-propulsion occurs unless pitch and heave are simultaneously present; (ii) a non-zero phase shift is required for the generation of net locomotion; and (iii) to achieve maximum velocity, $\phi \simeq \pm \pi/2$ is required. In the figures we present results for U_s , θ_o and ϕ as functions of the spring stiffness K for several values of the spring damping C from 0.1 to 10. All the plots are drawn for a given value of C, as a function of k^*/f^{*2} or K in dimensionless form, to ensure that all solutions collapse onto a single curve (see also Zhong *et al.* 2021). From figure 5 we may notice several results: first, the locomotion speed peaks at a specific value of K and, second, the

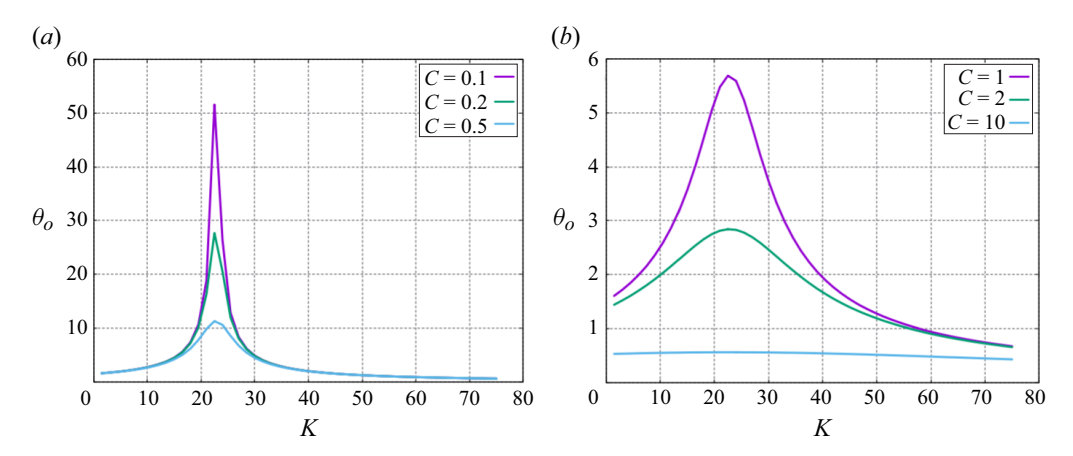


Figure 6. Pitch amplitude θ_0 as a function of K ($h_0 = 0.1$) for C = 0.1, 0.2, 0.5 (a); C = 1, 2, 10. (b).

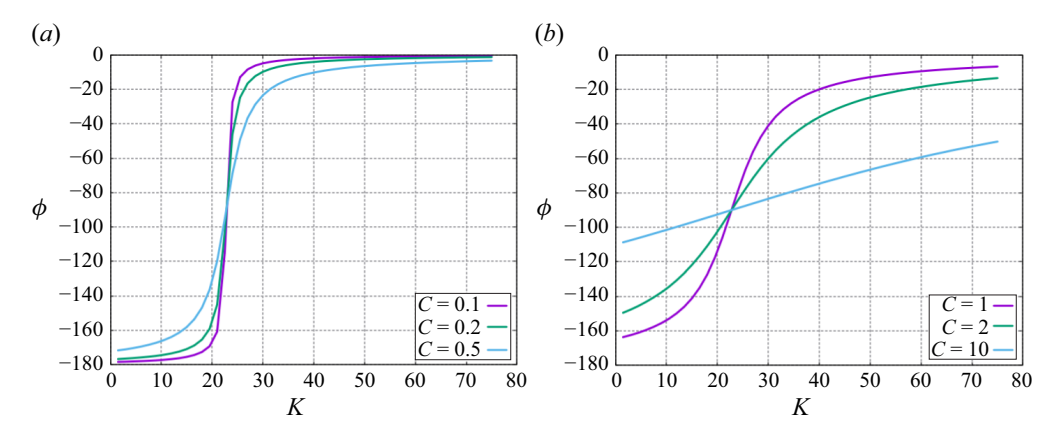


Figure 7. Phase angle variation as a function of K ($h_0 = 0.1$): (a) C = 0.1, 0.2, 0.5; (b) C = 1, 2, 10.

maximum value of the locomotion velocity increases as the spring damping decreases. This peak is likely a result of resonance effects, as discussed below.

The values of the pitch amplitude θ_o are reported in figure 6 as a function of K for several values of C. We notice both a peak at the same value of K as for the locomotion speed and a reduction in the amplitude for increasing C. Moreover, for C larger than one, the pitch amplitude quickly falls to very small values. On the contrary, for the smallest C it follows that θ_o exceeds the small-angle approximation, although a similar trend persists.

A comparison between active and passive motion reveals key differences. In the former case, the solution is given by (3.3) and shows a linear dependence of the velocity on both the amplitudes of heave h_o and pitch θ_o . On the other hand, in the passive case the pitch amplitude is not prescribed but is evaluated from the torsional balance. Equation (4.5) shows that θ_o is linearly dependent on h_o , leading to $U_s \propto h_o^2$. Both the physical coefficients of the spring balance, C and K, can also significantly affect the resulting pitch amplitude. Thus, we may argue that, to achieve optimal locomotion, these physical parameters should be tuned consistently to achieve the proper pitch amplitude.

The variation of the phase angle ϕ between pitch and heave is plotted in figure 7 as a function of K for the previously considered values of C. Notably, a steep change in ϕ occurs near the peak values of both U_s and θ_o . Specifically, by observing the peak

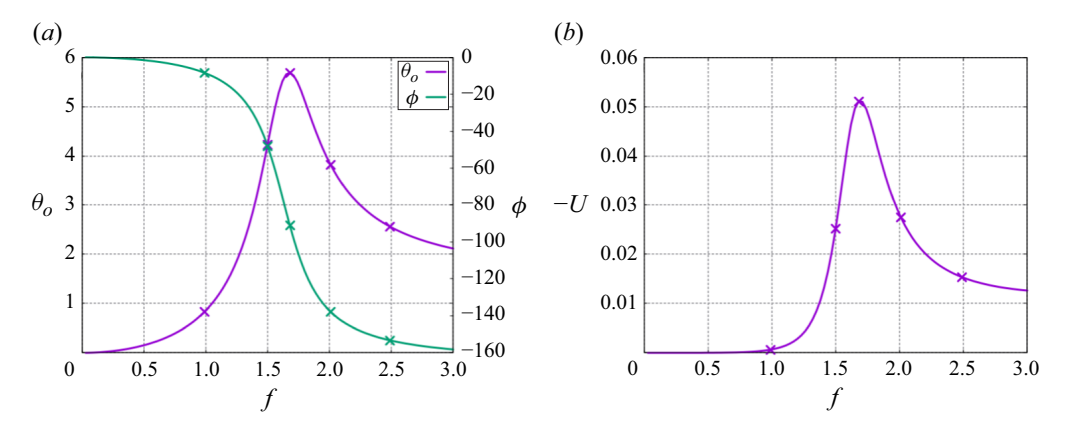


Figure 8. (a) Variation of θ_0 and ϕ as a function of frequency; (b) self-propulsion velocity $(h_0 = 0.1, k = 4000, C = 1)$.

values in figures 5 and 6 and by comparing with figure 7, we notice that, when U_s and θ_o reach their maximum values, it follows always that $\phi = -\pi/2$. In fact, from the second of (4.5), we notice that $\phi = \pm \pi/2$ for AA = 0 or, due to (4.7), $K = 4\pi^2 A_1$. By using the non-dimensional spring stiffness defined in (B4), the peak frequency occurs for

$$\frac{k^*}{f^{*2}} = K \,\rho^* \,b^{*4} = \rho^* \,b^{*4} \,4 \,\pi^2 \,A_1, \tag{4.9}$$

where A_1 depends on the mass ratio only, and its expression is reported in Appendix B. At the peak condition, i.e. for AA = 0, the torque balance equation shrinks to (see (B12))

$$C \dot{\theta} = BB h, \tag{4.10}$$

while the first expression in (4.5) yields

$$\theta_o = \frac{BB}{2\pi C} h_o. \tag{4.11}$$

Since the coefficient BB, defined in (4.6), is only function of the ratio between the body and the fluid mass, the pitch amplitude value increases without limits for vanishing spring damping C. Then, from (4.8), the self-propulsion speed is expressed as

$$U_s = -16 \pi^3 \frac{R (2 R + \pi)}{C (4 R + \pi)^2} h_o^2, \tag{4.12}$$

which also shows both the increase of the peak locomotion velocity for decreasing C and the relevance of h_o .

The pitch amplitude and phase and the opposite of the mean self-propulsion speed, $-U = -\overline{U_X^*}$, for C = 1 and k = 4000, are shown, as functions of the oscillation frequency, in figures 8(a) and 8(b), respectively. The values of θ_o and ϕ for some selected frequencies are used in figure 9 to represent the corresponding stroke loop in the shape space (i.e. where the variables h and θ , which describe the shape of the body, are the independent variables). We notice that the area of each curve increases with the mean self-propulsion speed, while its orientation is only related to the phase angle. For vanishing ϕ , a reciprocal motion is obtained, which gives null locomotion. On the contrary, the curve with the largest area in the shape space corresponds to the maximum locomotion speed and to a

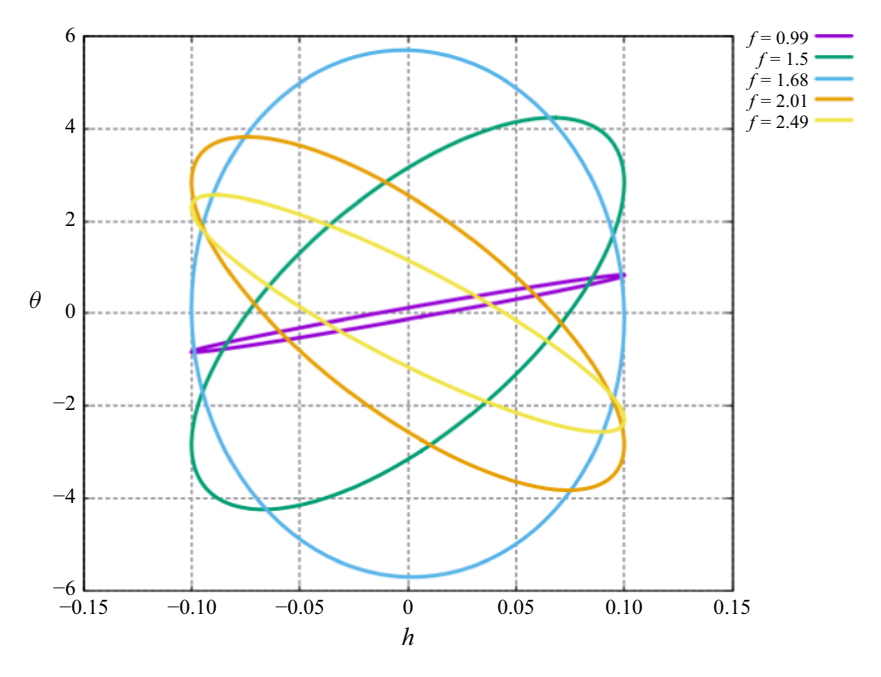


Figure 9. Stroke loops in the shape space for the frequencies selected in figure 8 ($h_0 = 0.1$, k = 4000, C = 1).

phase shift $-\pi/2$. These results confirm the observations of other authors (see e.g. Ross 2006, Hatton & Choset 2010).

Several solutions reported above for the passive swimming plate display a peaky behaviour which resembles that of the amplification factor of a forced harmonic oscillator with damping.

The peak frequency given by (4.9) is related to the natural oscillation frequency defined by (B19). From this expression we obtain $k^*/f_N^{*2} = 4\pi^2 \rho^* b^{*4} A_1$, as given by (4.9), confirming that the peak locomotion speed occurs at the natural frequency with a clear connection to resonance phenomena (see Beal *et al.* 2006, Michelin & Smith 2009, Alben *et al.* 2012, Moore 2014, Paraz, Schouveiler & Eloy 2016, Lopez-Tello, Fernandez-Feria & Sanmiguel-Rojas 2023). The damping term was not accounted for in the above evaluation of the natural frequency, since it has a negligible effect.

5. Concluding remarks

The results presented in this paper provide a further contribution to clarify the question raised by Saffman more than 50 years ago regarding swimming in a perfect fluid. Namely, if we consider a deformable body in a quiescent perfect fluid, we find that a self-propulsion may occur through the exchange of reactive forces with the surrounding fluid, without any generation or release of vorticity, provided that a proper deformation is prescribed. Our study focuses on fish locomotion driven by a tail flapping, while the main body contributes only inertial effects, as no resistive forces are considered. This oscillatory swimming model is representative of tuna or other species within the broader class of carangiform fish. Similar configurations can be effectively analysed using a simplified model consisting of a virtual body with an oscillating tail attached to its end to generate the propulsion for the entire fish. This approximation provides a direct answer to the fundamental question

of whether a fish can achieve locomotion solely through appropriate body deformation, without the release of vorticity.

To investigate this phenomenon, we adopted an impulse-based mathematical model that considers only added-mass forces in a purely potential flow. As a preliminary case, we analysed active oscillations in which heave and pitch motions are fully prescribed. A flat plate was used as the geometric model for the tail, allowing analytical solutions to provide global results without caring about singular behaviour at the plate's sharp edges in the absence of viscosity The results confirm that self-propulsion is generated by the flapping tail, provided a phase shift between heave and pitch is established, and, if one of these motions is prevented, no self-propulsion takes place. Even in this relatively simple case, despite several results already available in the literature, the topic of locomotion in a perfect fluid still raises some perplexities. We hope that our findings for a simple fish-like configuration may help to further clarify this issue.

The aim of the paper is to consider more realistic configurations accounting for the flexibility of the tail. In this case, the pitch amplitude and phase lag are no longer prescribed, but instead emerge from fluid–structure interaction. Within this framework, the tail motion is passive and requires an additional torque balance equation to capture its flexibility, which we model as being concentrated at the LE via a torsional spring. Notice that a localised torsional spring with tuneable stiffness is considered one of the most effective approaches for assessing the role of flexibility in the passive tail dynamics. A more detailed analysis was required to balance all torques acting about the rotation centre, located at the peduncle that connects the tail to the main body. Structural damping must also be taken into account, in addition to fluid–structure interaction. In this context, the phase shift, previously shown to be essential for locomotion, emerges as a result of structural damping, which may become negligible in a complete solution where damping due to vortex shedding dominates.

The solution for the flexible tail reveals the key result: a unique relationship between stride length and non-dimensional stiffness. This relationship displays a characteristic growth pattern at a specific value of non-dimensional stiffness, corresponding to the natural frequency of the tail foil in an otherwise quiescent fluid.

To maintain an optimal stride length, a fish swimming at a given frequency must adjust its stiffness through muscular action in the peduncle region. Alternatively, for a fixed stiffness, the fish must tune its swimming frequency to maximise performance. This result closely mirrors self-propulsion mechanisms observed in nature. In essence, the fish must fine tune its physical parameters to achieve a stride length that aligns with the resonance region.

Finally, extending this study to more realistic conditions – including circulatory forces and vorticity shedding, for instance, by means of a Kutta condition – will be greatly facilitated by our current approach. The proposed methodology ensures precise control over the critical components of the solution associated with pure inertial terms. In contrast, the inclusion of vortical impulse and vorticity release tends to dominate the resulting dynamics, potentially obscuring the more subtle aspects addressed in this paper. A further deepening on this matter is firmly envisaged by the authors to strengthen the above conceptual points.

Acknowledgements. The research of G.G. was founded by Sapienza University of Rome through the research grant 'Progetti di Ricerca 2023 N.RP123188E86CE50C'. This work was produced externally to Leonardo S.p.A. and does not involve any proprietary data, information or projects. We also thank the anonymous referee for the many helpful remarks.

Declaration of interests. The authors report no conflict of interest.

Author contributions. All authors contributed equally to this work.

Appendix A. Forces and moment

According to Newman (2017), we may express the forces acting on the body within an acyclic potential flow. Let us denote the translation velocity of LE as $U_o(t) = \{U_1e_1; U_2e_2; \}$ or, by defining r the radius vector with origin in LE, $V_B = U_o + \Omega e_3 \times r$.

The potential ϕ satisfies Laplace's equation with the boundary condition on the body contour

$$\frac{\partial \phi}{\partial n} = V_B \cdot n = U_o \cdot n + \Omega (r \times n) \cdot e_3. \tag{A1}$$

We split the potential into the basis potentials $\phi = \phi_i U_i$ with i = 1, 2, 3. Here, ϕ_i represents the velocity potential due to a body motion with unit velocity U_i in the *i*th mode (linear $U_i = U(t)$ for i = 1,2 or angular for $U_3 = \Omega(t)e_3$). These basis motions and their time derivatives (U_i and \dot{U}_i) are considered in the body frame

$$\phi = U_1 \,\phi_1 + U_2 \,\phi_2 + U_3 \,\phi_3 = U_i \,\phi_i \quad i = 1, 2, 3. \tag{A2}$$

By substituting (A2) into (A1) it follows that

$$U_1 \frac{\partial \phi_1}{\partial n} + U_2 \frac{\partial \phi_2}{\partial n} + U_3 \frac{\partial \phi_3}{\partial n} = U_1 n_1 + U_2 n_2 + U_3 (\mathbf{r} \times \mathbf{n})_3.$$
 (A3)

Each one of the potentials ϕ_i satisfies Laplace's equation, the vanishing condition at infinity and the condition on the body contour

$$\frac{\partial \phi_1}{\partial n} = n_1 \quad \frac{\partial \phi_2}{\partial n} = n_2 \quad \frac{\partial \phi_3}{\partial n} = (\mathbf{r} \times \mathbf{n})_3. \tag{A4}$$

In the body-fixed reference frame, the potentials ϕ_i depend only on the geometry of the body (through the normal n) and not on time or the velocities U_i . In the ground frame, the force acting on the body, by substituting (A2) into (2.6), is expressed as

$$\mathbf{F_b} = \rho \frac{d}{dt} \left(U_i(t) \int_{S_b} \phi_i \mathbf{n} \, dS \right), \tag{A5}$$

where the integral depends on time due to the variation of n caused by the rotation of the body: $dn/dt = \Omega \times n$. From (A5), the force components in the body frame, expressed in index form, are

$$F_{j} = \rho \,\dot{U}_{i}(t) \int_{S_{h}} \phi_{i} n_{j} \,dS + \rho \,\epsilon_{j3l} U_{i} \Omega \int_{S_{h}} \phi_{i} n_{l} \,dS \quad i, l = 1, 2, 3 \quad j = 1, 2, \quad (A6)$$

where ϵ_{ijk} is the permutation tensor. By considering the boundary conditions (A4), the above appearing integrals may be evaluated as

$$\rho \int_{S_b} \phi_i n_j \, dS = \rho \int_{S_b} \phi_i \frac{\partial \phi_j}{\partial n} \, dS = -m_{ji}, \tag{A7}$$

where m_{ji} are the components of the added-mass tensor whose values depend solely on the geometry of the body. When considering a flat plate with length 2 b (zero thickness) pitching about its LE, the only non-zero added-mass coefficients (including also $m_{3\,3}$ appearing in the following) are

$$m_{22} = \rho \pi b^2$$
 $m_{23} = \rho \pi b^3$ $m_{33} = \frac{9}{8} \pi \rho b^4$. (A8)

According to (A6), by using F_x and F_y instead of F_1 and F_2 , the force components in the body-fixed frame may be written as

$$\begin{cases} F_x = \Omega(m_{21}U_1 + m_{22}U_2 + m_{23}\Omega) = \rho\pi b^2 \Omega(U_2 + b \Omega), \\ F_y = -(m_{21}\dot{U}_1 + m_{22}\dot{U}_2 + m_{23}\dot{\Omega}) = -\rho\pi b^2(\dot{U}_2 + b \dot{\Omega}). \end{cases}$$
(A9)

Similarly, by using the basis potentials, the impulse components can be expressed as

$$\begin{cases} \rho P_x = -\rho \int_{S_b} \phi n_x \, dS = -\rho \int_{S_b} U_i \, \phi_i n_x \, dS = m_{11} U_1 + m_{12} U_2 + m_{13} \Omega, \\ \rho P_y = -\rho \int_{S_b} \phi n_y \, dS = -\rho \int_{S_b} U_i \, \phi_i n_y \, dS = m_{21} U_1 + m_{22} U_2 + m_{23} \Omega. \end{cases}$$
(A10)

It follows for the flat plate

$$\begin{cases}
P_x = 0, \\
P_y = \pi b^2 (U_2 + b \Omega).
\end{cases}$$
(A11)

Finally, the forces can be expressed in terms of the impulses as

$$\begin{cases}
F_x = \rho \frac{d}{dt} \int_{S_b} \phi n_x \, dS - \rho \Omega \int_{S_b} \phi n_y \, dS = \rho \Omega P_y, \\
F_y = \rho \frac{d}{dt} \int_{S_b} \phi n_y \, dS + \rho \Omega \int_{S_b} \phi n_x \, dS = -\rho \frac{dP_y}{dt}.
\end{cases} (A12)$$

By following the same approach as above, the fluid dynamic moment is given by

$$M_{j} = \rho \dot{U}_{i} \int \phi_{i} (\mathbf{r}' \times \mathbf{n})_{j} dS + \rho \epsilon_{jkl} U_{i} U_{k} \int \phi_{i} n_{l} dS \qquad i = 1, 2, 3.$$
 (A13)

The boundary condition on the body contour is expressed as in (A1) with r' instead of r, while each one of the basis potentials ϕ_i satisfies the condition (A4). In the present two-dimensional solution, the only non-vanishing component of the moment is M_3 , which follows from (A13)

$$M_3 = \rho \left(\dot{U}_i \int \phi_i \, (\mathbf{r'} \times \mathbf{n})_3 \, \mathrm{d}S + U_i \, U_1 \int \phi_i n_2 \, \mathrm{d}S - U_i \, U_2 \int \phi_i n_1 \, \mathrm{d}S \right) \quad i = 1, 2, 3. \tag{A14}$$

By using (A7) and introducing further components of the added-mass matrix

$$\rho \int \phi_i (\mathbf{r'} \times \mathbf{n})_3 \, \mathrm{d}S = \rho \int_{S_b} \phi_i \frac{\partial \phi_3}{\partial n} \, \mathrm{d}S = -m_{3i} \quad i = 1, 2, 3.$$
 (A15)

Equation (A14) gives, writing Ω for U_3 ,

$$M_3 = -\dot{U}_1 m_{13} - \dot{U}_2 m_{23} - \dot{\Omega} m_{33} - U_1^2 m_{12} - U_2 U_1 m_{22} - \Omega U_1 m_{32} + U_1 U_2 m_{11} + U_2^2 m_{21} + \Omega U_2 m_{31},$$
(A16)

which, for the flate plate, can be simplified into

$$M_{3} = -\dot{U}_{2}m_{23} - \dot{\Omega}m_{33} - U_{2}U_{1}m_{22} - \Omega U_{1}m_{32}$$

$$= -\pi \rho b^{2} \left[b \dot{U}_{2} + \frac{9}{8}b^{2}\dot{\Omega} + U_{2}U_{1} + b \Omega U_{1} \right], \tag{A17}$$

where m_{23} and m_{33} relate fluid inertia to heave and pitch, while m_{22} and m_{32} introduce nonlinear effects due to added-mass coupling. Let us recall that U_1 and U_2 are the LE translation velocities in the body frame of reference.

Appendix B. Non-dimensional torque balance equation and pitch solution

We consider a thin flat plate with thickness s^* , length c^* and density ρ_b^* . The semichord $b^* = c^*/2$ is chosen as the reference length. The total mass of the plate is given by $m_p^* = \rho_p^* s^* c^*$. As previously defined, dimensional quantities are denoted with an asterisk (*), while dimensionless variables appear without one. We introduce the following nondimensional quantities x, h, t, among others. Specifically we define $x = x^*/b^*$, $h = h^*/b^*$ and $t = t^* / T^*$.

In order to estimate the mass of the body, we assume, as previously defined in Paniccia et al. (2021c), that the length of the total body (virtual + tail) is L^* ; that the length of the tail is $c^* = L^*/7$; and that the virtual body may be represented by an elliptical shape with chord $c_b^* = (6/7)$ $L^* = 6$ c^* , 4% thickness with $s_b^* = 0.04$ $c_b^* = 0.24$ c^* . So the area of the virtual body is $V_b^* = \pi(c_b^* s_b^*/4) = 0.36\pi c^{*2}$ and $m_b^* = \rho_b^* V_b^*$. The equation governing passive flapping motion, in its dimensional form, is

$$I^* \ddot{\theta}^* + C^* \dot{\theta}^* + k^* \theta^* = M_f^* + M_i^*, \tag{B1}$$

where θ has been defined in (3.1). The moment of inertia about the LE is $I^* = (8/3)\rho_b^* s^* b^{*3}$ while C^* and k^* represent the structural damping coefficient and the torsional stiffness of the spring, respectively. Here, M_f^* is the fluid dynamic moment acting on the foil's LE and M_i^* is the inertial torque caused by the vertical acceleration of the LE. (i.e. the pitching pivot point) during flapping.

To obtain the non-dimensional form of (B1) we divide all terms by $\rho b^{*2} V_p^{*2}$, where $V_R^* = b^* f^*$ is the reference velocity. The non-dimensionalised inertia term becomes

$$\frac{I^* \ddot{\theta}^*}{\rho b^{*4} f^{*2}} = \frac{8}{3} \frac{\rho_b^* s^* b^{*3} \ddot{\theta}^*}{\rho b^{*4} f^{*2}} = \frac{16}{3} \frac{\rho_b^* s^*}{\rho^* c^*} \ddot{\theta} = \frac{16}{3} R \ddot{\theta}, \tag{B2}$$

where $R = s^* \rho_h^*/c^* \rho^*$ is the ratio of body to fluid inertia. Similarly, the non-dimensional damping term is

$$\frac{C^* \dot{\theta}^*}{\rho^* b^{*4} f^{*2}} = \frac{C^* f^* \dot{\theta}}{\rho^* b^{*4} f^{*2}} = C \dot{\theta} \quad \text{where} \quad C = \frac{C^*}{\rho^* b^{*4} f^*}. \tag{B3}$$

The coefficient of the spring restoring torque is expressed as

$$\frac{k^*}{\rho^* b^{*4} f^{*2}} = K. \tag{B4}$$

In this form, according to (B4), the spring effect, through K, appears to be related to the ratio $k^*/f_{..}^{*2}$. The inertial moment due to the forced heaving motion of the body, $M_i^* = -m_n^* b^* \ddot{h}^*$, may be expressed in non-dimensional form as

$$M_i = \frac{M_i^*}{\rho^* b^{*4} f^{*2}} = 8\pi^2 \frac{\rho_b^* s^*}{\rho^* b^*} h = 16\pi^2 R h.$$
 (B5)

The corresponding expression of the fluid dynamic moment is obtained by introducing in (4.3) the above defined non-dimensional quantities

$$M_f = \frac{M_f^*}{\rho \ b^{*4} \ f^{*2}} = -\pi \left\{ CC \ddot{h} + \left[CC + \frac{1}{8} \right] \ddot{\theta} \right\},\tag{B6}$$

where the non-dimensional coefficient CC is defined as

$$CC = \frac{m_p^*}{m_p^* + \pi \ \rho^* \ b^{*2}} = \frac{1}{1 + \frac{\pi}{4} \frac{\rho^* \ c^*}{\rho_p^* \ s^*}} = \frac{4 \ R}{4 \ R + \pi}.$$
 (B7)

The final non-dimensional form of the torque balance (B1) is

$$\frac{16}{3}R\ddot{\theta} + C\dot{\theta} + K\theta = M_f + M_i, \tag{B8}$$

which can be recast, by using the above reported expressions for M_i and M_f , as

$$\left[\frac{16}{3}R + \pi \left(CC + \frac{1}{8}\right)\right]\ddot{\theta} + C\dot{\theta} + K \theta = -\pi CC \ddot{h} + 16\pi^2 R h, \tag{B9}$$

or restated in a more concise form as

$$A_1 \ddot{\theta} + C\dot{\theta} + K \theta = -\pi CC \ddot{h} + 16\pi^2 R h,$$
 (B10)

where

$$A_1 = \left[\frac{16}{3} R + \pi \left(CC + \frac{1}{8} \right) \right]. \tag{B11}$$

Equation (B10) can be rearranged, by using the harmonic expressions for $\ddot{\theta}$ and \ddot{h} and by defining two further non-dimensional coefficients AA and BB, as

$$AA\theta + C\dot{\theta} = BBh, \tag{B12}$$

where

$$AA = -4\pi^2 A_1 + K = -\frac{64}{3}\pi^2 R + K - \pi^3 \left(\frac{36 R + \pi}{8 R + 2 \pi}\right), \tag{B13}$$

$$BB = 4\pi^{3}CC + 16\pi^{2}R = 16\pi^{2}R \left[\frac{4R + 2\pi}{4R + \pi}\right].$$
 (B14)

Finally, by using standard manipulations, the solution for the passive pitch motion is obtained in terms of θ_0 and ϕ

$$\begin{cases} \theta_o = \frac{BB h_o}{\sqrt{AA^2 + 4\pi^2 C^2}}, \\ \tan(\phi) = \frac{-2\pi C}{AA}. \end{cases}$$
(B15)

Equation (B15) allows for several observations: (i) the phase angle increases with C and reaches its maximum when AA = 0; (ii) the pitch amplitude vanishes for BB = 0, i.e. for a massless body, and is otherwise inversely related to C.

The passive flapping motion is described by (B1), which corresponds to a damped system with harmonic forcing. Therefore, a natural frequency may be evaluated which is related to a resonant behaviour. We have expressed the fluid dynamic torque in (4.3) which is here restated in a more concise form as

$$M_f^* = M_h^* \ddot{h}^* + M_\theta^* \ddot{\theta}^*,$$
 (B16)

where

G. Graziani, D. Paniccia and R. Piva

$$M_h^* = -\pi \rho^* b^{*3} C C \quad M_\theta^* = -\pi \rho^* b^{*4} \left[C C + \frac{1}{8} \right],$$
 (B17)

and CC is defined in (B7).

Let us assume no heave forcing (i.e. $M_h^* = 0$) and $M_i^* = 0$. Now (B1), by developing time derivatives, becomes

$$-\omega^{*2}(I^* - M_{\theta}^*) + i \ \omega^* C^* + k^* = 0.$$
 (B18)

The undamped natural frequency of torsional vibration in vacuum depends on the spring stiffness k^* as well as on the moment of inertia about the LE I^* : $\omega_v^* = \sqrt{k^*/I^*}$ The presence of the fluid modifies this frequency and from (B18) we obtain

$$\omega_N^* = \sqrt{\frac{k^*}{I^* - M_\theta^*}} = \sqrt{\frac{k^*}{\rho^* b^{*4} A_1}}.$$
 (B19)

Appendix C. Kinetic energy

The kinetic energy (T) of the isolated fluid-body system may be expressed through the sum of the kinetic energy of the body and of the fluid

$$T_{body} = \frac{1}{2}m_b(u_y + \dot{h})^2 + \frac{1}{2}I_{zz}\dot{\theta}^2.$$
 (C1)

The kinetic energy of the fluid may be expressed in terms of the added mass and of the base velocities (see e.g. Childress 1981; Newman 2017)

$$T_{fluid} = \frac{1}{2} m_{ij} U_i U_j = \frac{1}{2} \left[m_{22} (u_y + \dot{h})^2 + m_{33} \dot{\theta}^2 + 2 m_{23} (u_y + \dot{h}) \dot{\theta} \right], \tag{C2}$$

which may be added to give

$$T = \frac{1}{2} \left[(m_b + m_{22})(u_y + \dot{h})^2 + (I_{zz} + m_{33})\dot{\theta}^2 \right] + m_{23}(u_y + \dot{h})\dot{\theta}.$$
 (C3)

As discussed in Kanso (2009), the total kinetic energy could be split into three contributions: one related to the shape deformation $(\dot{h} \text{ and } \dot{\theta})$, one related to the body locomotion (u_y) and the remaining one acting as a coupling effect between both of them. In her case of a massless body it can be shown that most of the energy input into the fluid by the deformation is transformed in locomotion energy.

Here, we consider how the overall energy of the fluid is distributed between that of the fluid, T_{fluid} given by (C2), and that of the body's motion, T_{body} given by (C1). When the surface of the body is periodically deformed due to the effect of some internal mechanism, the momentum of the body+fluid system changes and both these contributions are periodically oscillating in time. In the absence of shed vorticity, no energy is transferred to the wake, hence the total energy displays periodic oscillations with a constant non-zero mean value. On the contrary, in the presence of wake release, the mean value of the total energy increases with time. Each one of the above reported expressions is shown in figure 10 during one cycle.

In figure 11 we show the behaviour during one cycle of each one of the three parts of the total kinetic energy appearing in (C3). We notice that the first two terms are always positive, while the third one, representing the coupling between heave and pitch, has a negative mean value.

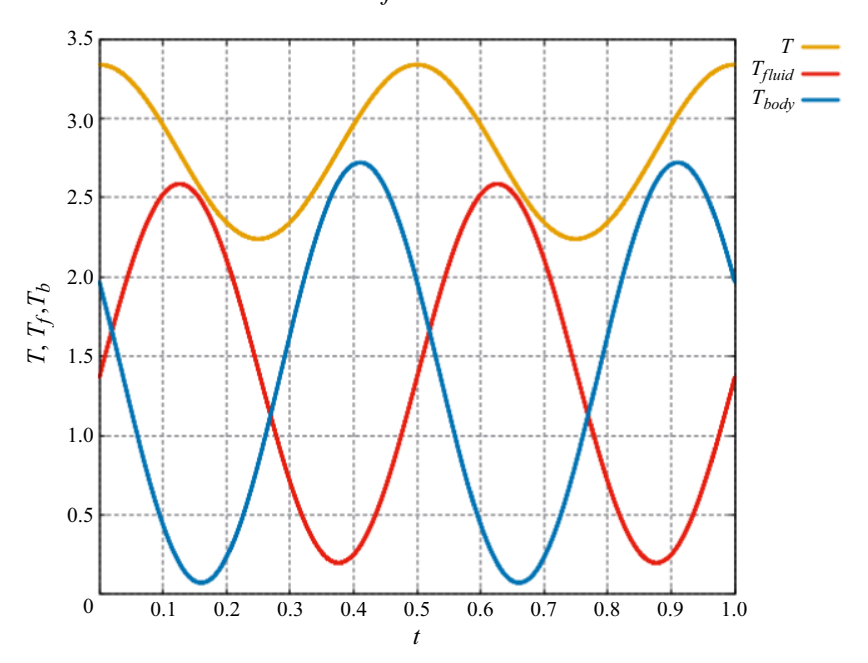


Figure 10. Time behaviour of total kinetic energy $T=T_{body}+T_{fluid}$ and partial contributions $T_{body},\,T_{fluid}$ for $m_b\neq 0,\,h_o=0.1,\,\theta_o=10^\circ,\,\phi=-90^\circ.$

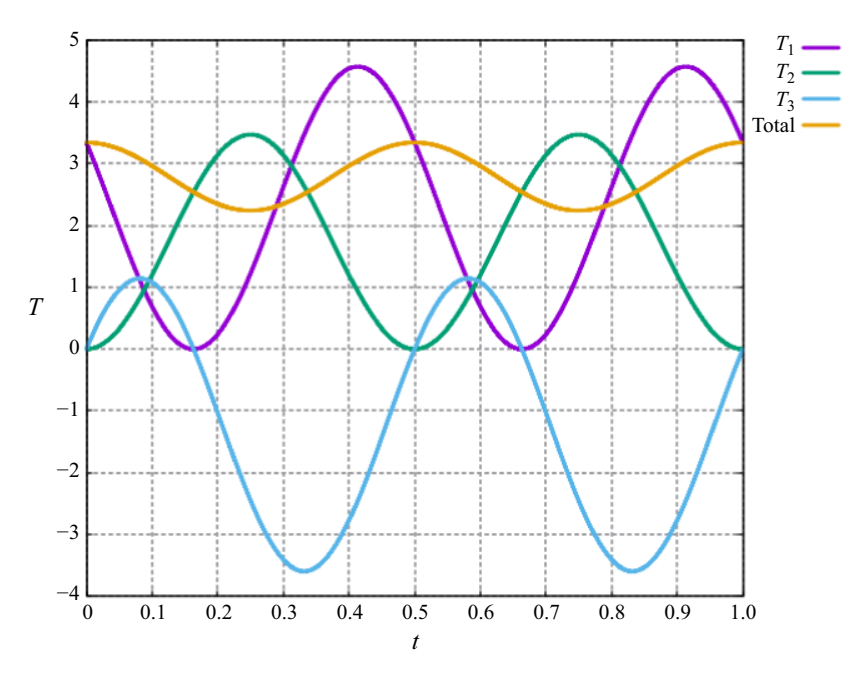


Figure 11. Time behaviour of the separate contributions to the total kinetic energy appearing in (C3) for $m_b \neq 0$, $h_o = 0.1$, $\theta_o = 10^\circ$, $\phi = -90^\circ$. Here, $T_1 = (1/2)(m_b + m_{22})(u_y + \dot{h})^2$, $T_2 = (1/2)(I_{zz} + (9/8)m_{22}b^2)\dot{\theta}^2$, $T_3 = b\dot{\theta}m_{22}(u_y + \dot{h})$.

G. Graziani, D. Paniccia and R. Piva

REFERENCES

- AKOZ, E. & MOORED, K.W. 2018 Unsteady propulsion by an intermittent swimming gait. *J. Fluid Mech.* **834**, 149–172
- ALBEN, S., WITT, C., BAKER, T.V., ANDERSON, E. & LAUDER, G.V. 2012 Dynamics of freely swimming flexible foils. *Phys. Fluids* 24, 051901.
- BATCHELOR, G.K. 1991 An Introduction to Fluid Dynamics Cambridge University Press
- BEAL, D.N., HOVER, F.S., TRIANTAFYLLOU, M.S., LIAO, J.C. & LAUDER, G.V. 2006 Passive propulsion in vortex wakes. *J. Fluid Mech.* **549**, 385–402.
- CHAMBRION, T. & MUNNIER, A. 2011 Locomotion and control of a self-propelled shape-changing body in a fluid. *J. Nonlinear Sci.* 21, 325–385.
- CHILDRESS, S. 1981 Mechanics of Swimming and Flying. Cambridge University Press, Cambridge, USA.
- CHILDRESS, S. & DUDLEY, R. 2004 Transition from ciliary to flapping mode in a swimming mollusc: flapping flight as a bifurcation in Re_{ω} . J. Fluid Mech. **498**, 257–288.
- ELDREDGE, J.D. 2019 Mathematical Modeling of Unsteady Inviscid Flows, vol. 50. Springer Intern. Publ., Cham, Switzerland.
- ELDREDGE, J.D., TOOMEY, J. & MEDINA, A. 2010 On the roles of chord-wise flexibility in a flapping wing with hovering kinematics. *J. Fluid Mech.* **659**, 94–115.
- HANG, H., HEYDARI, S., COSTELLO, J.H. & KANSO, E. 2022 Active tail flexion in concert with passive hydrodynamic forces improves swimming speed and efficiency. *J. Fluid Mech.* 932, A35.
- HATTON, R.L. & CHOSET, H. 2010 Connection vector fields and optimized coordinates for swimming systems at low Reynolds numbers. In Proc. ASME 2010 Dynamic Systems and Control Confer. (DSCC 2010), ASME pp. 1–8.
- KANSO, E. 2009 Swimming due to transverse shape deformations. J. Fluid Mech. 631, 127-148.
- KANSO, E., MARSDEN, J.E., ROWLEY, C.W. & MELLI-HUBER, J.B. 2005 Locomotion of articulated bodies in a perfect fluid. *J. Nonlinear Sci.* 15, 255–289.
- KELLY, S.D. & MURRAY, R.M. 2000 Modelling efficient pisciform swimming for control. *Int. J. Robust Nonlinear Control* 10, 217–241.
- KELLY, S.D. 1998 The mechanics and control of robotic locomotion with applications to aquatic vehicles PhD thesis. California Institute of Technology.
- LIGHTHILL, J. 1960 Note on the swimming of slender fish. J. Fluid Mech. 9 (2), 305-317.
- LIGHTHILL, J. 1969 Hydromechanics of aquatic animal propulsion: a survey. Annu. Rev. Fluid Mech. 1, 413–446.
- LIMACHER, E.J. 2019 Added mass and vortical impulse: theory and experiment *PhD thesis*. University of Calgary.
- LIMACHER, E.J. 2021 Added-mass force on elliptic airfoils. J. Fluid Mech. 926, R2.
- LOPEZ-TELLO, P.E., FERNANDEZ-FERIA, R. & SANMIGUEL-ROJAS, E. 2023 Efficient self-propelled locomotion by an elastically supported rigid foil actuated by a torque. *Appl. Mathem. Modell.* **116**, 236–253.
- MASON, R. 2003 Fluid locomotion and trajectory planning for shape-changing robots PhD thesis. California Institute of Technology.
- MELLI, J.B., ROWLEY, C.W. & RUFAT, D.S. 2006 Motion planning for an articulated body in a perfect planar fluid. SIAM J. Appl. Dyn. Syst. 5, 650–669.
- MICHELIN, S. & SMITH, S.G.L. 2009 Resonance and propulsion performance of a heaving flexible wing. *Phys. Fluids* **21**, 071902.
- MILOH, T. & GALPER, A. 1993 Self-propulsion of general deformable shapes in a perfect fluid. Proc. R. Soc. Lond. A 442, 273–299.
- MOORE, M.N.J. 2014 Analytical results on the role of flexibility in flapping propulsion. *J. Fluid Mech.* **757**, 559–612.
- MOORE, M.N.J. 2015 Torsional spring is the optimal flexibility arrangement for thrust production of a flapping wing. *Phys. Fluids* **27**, 091701.
- MOORED, K.W. & QUINN, D.B. 2019 Inviscid scaling laws of a self-propelled pitching airfoil. AIAA J. 57 (9), 3686–3700.
- NEWMAN, J.N. 2017 Marine Hydrodynamics. MIT Press, Cambridge, USA.
- PANICCIA, D., GRAZIANI, G., LUGNI, C. & PIVA, R. 2021a On the role of added mass and vorticity release for self propelled aquatic locomotion. *J. Fluid Mech.* 918, A45.
- PANICCIA, D., GRAZIANI, G., LUGNI, C. & PIVA, R. 2021b The relevance of recoil and free swimming in aquatic locomotion. *J. Fluids Struct.* **103**, 103290.
- PANICCIA, D., GRAZIANI, G., LUGNI, C. & PIVA, R. 2022 The fish ability to accelerate and suddenly turn in fast maneuvers. Sci. Rep. 12, 4946.

- PANICCIA, D., PADOVANI, L., GRAZIANI, G. & PIVA, R. 2021c The performance of a flapping foil for a self-propelled fishlike body. *Sci. Rep.* 11, 22297.
- PANICCIA, D., PADOVANI, L., GRAZIANI, G. & PIVA, R. 2023 Locomotion performance for oscillatory swimming in free mode. *Bioinspir. Biomim.* 18, 015004.
- PARAZ, F., SCHOUVEILER, L. & ELOY, C. 2016 Thrust generation by a heaving flexible foil: resonance nonlinearities and optimality. *Phys. Fluids* 28, 011903.
- PURCELL, E.M. 1977 Life at low Reynolds number. Am. J. Phy. 45 (1), 3-11.
- QUINN, D.B. & LAUDER, G.V. 2022 Tunable stiffness in fish robotics: mechanisms and advantages. *Bioinspir. Biomim.* 17, 011002.
- QUINN, D.B., LAUDER, G.V. & SMITS, A.J. 2015 Maximizing the efficiency of a flexible propulsor using experimental optimization. *J. Fluid Mech.* 767, 430–448.
- RADFORD, J.E. 1998 Symmetry reduction and swimming in a perfect fluid PhD thesis. California Institute of Technology.
- Ross, S.D. 2006 Optimal flapping strokes for self-propulsion in a perfect fluid. In *Proc. American Control Confer. IEEE*, ThC18.3, pp. 4118–4122
- SAFFMAN, P.G. 1967 The self-propulsion of a deformable body in a perfect fluid. *J. Fluid Mech.* 28 (2), 385–389.
- SAFFMAN, P.G. 1992 Vortex Dynamics Cambridge University Press.
- SMITS, A.J. 2019 Undulatory and oscillatory swimming. J. Fluid Mech. 874, 1-70.
- SPAGNOLIE, S.E., MORET, L., SHELLEY, M.J. & ZHANG, J. 2010 Surprising behaviors in flapping locomotion with passive pitching. *Phys. Fluids* 22 (4), 041903.
- THEODORSEN, T. 1935 General theory of aerodynamic instability and the mechanism of flutter. Tech. Rep.
- TOOMEY, J. & ELDREDGE, J. 2008 Numerical and experimental study of the fluid dynamics of a flapping wing with low order flexibility. *Phys. Fluids* **20** (7), 073603.
- VAN BUREN, T., FLORYAN, D. & SMITS, A.J. 2018 Scaling and performance of simultaneously heaving and pitching foils. AIAA J. 57 (9), 1–12.
- VANELLA, M., FITZGERALD, T., PREIDIKMAN, S., BALARAS, E. & BALACHANDRAN, B. 2009 Flapping wing structural deformation and thrust correlation study with flexible membrane wings. *J. Exper. Biol.* 212 (1), 95–105.
- WAN, H., DONG, H. & HUANG, G.P. 2012 Hovering hinge-connected flapping plate with passive deflection. *AIAA J.* **50** (9), 2020–2026.
- Wu, T.Y. 1971 Hydromechanics of swimming propulsion. Part 1: swimming of 2D flexible plate at variable forward speed inviscid fluid. J. Fluid Mech. 46, 337–355.
- Wu, T.Y. 1961 Swimming of a waving plate. J. Fluid Mech. 10 (3), 321-344.
- ZHANG, J., LIU, N.S. & LU, X.Y. 2010 Locomotion of a passively flapping flat plate. *J. Fluid Mech.* **659**, 43–68.
- ZHONG, Q., ZHU, J., FISH, F.E., KERR, S.J., DOWNS, A.M., BART-SMITH, H. & QUINN, D.B. 2021 Tunable stiffness enables fast and efficient swimming in fish-like robots. *Sci. Robot.* 6, eabe4088.